Experimental Investigation and Modelling of Laser Machining of Sapphire for High Temperature Pressure Transducers

Justin Collins* William Oates†

Florida Center for Advanced Aero Propulsion (FCAAP)

Department of Mechanical Engineering

Florida A & M and Florida State University

Tallahassee, FL, 32310, USA

Daniel Blood‡ David Mills§ Mark Sheplak¶

Department of Mechanical and Aerospace Engineering

University of Florida

Gainesville, Fl 32611-6250

Sensing of pressure at high temperatures is currently limited by melting temperature and the plastic deformation undergone by silicon based technologies due to brittle to ductile transition.[1] Sapphire has been proposed as an alternative sensing material that can overcome these temperature limitations using photonic methods. In order to manufacture the sensors, an ultra-short pulsed laser is utilized to machine sapphire as opposed to chemical etching methods used in silicon-based MEMS technology. Here we quantify the change in mechanical properties of sapphire due to laser machining. Vicker's indentations were applied to both pristine and laser machined specimens showing that there is a toughening effect due to the machining process. The underlying mechanisms associated with toughening were quantified using transmission electron microscopy (TEM) and a single crystal plasticity model using finite element analysis. The TEM cross-sections illustrated dense sub-surface regions of dislocations only in laser machined specimens. To further understand the toughening, finite element modeling of nanoindentations were conducted and compared with data illustrating complex evolution of the single crystal sapphire material underneath the nanoindent. The modeling and data comparison suggest hardening occurs locally that can be associated with an increase in the elastic properties as well as local damage.

Nomenclature

F_{iK}	Deformation gradient
$\tilde{T}_{IJ}$	2^{nd} Piola-Kirchoff stress
ρ	Damage internal state variable
ξ_i	Damage microforce
η	Internal microscopic potential
β	Inverse mobility constant
s_i	Slip direction unit vector
m_j	Slip plane unit normal

*Research Assistant, jmc07g@my.fsu.edu

†Associate Professor, woates@fsu.edu, AIAA member

‡Research Assistant, daniel.blood@ufl.edu

§Post Doctoral Researcher, dm82@ufl.edu

¶Professor, sheplak@ufl.edu

I. Introduction

Sapphire is known for its unique properties including extreme hardness (only natural substance harder than it is diamond) and high melting temperature (2030^oC).[2] Sapphire is utilized in both structural and functional applications due to advantages pertaining to mechanical, thermal, and chemical properties. Resistance to thermomechanical degradation and chemical corrosion makes it an ideal material for applications in hostile aerospace environments such as rocket nose cones and gas turbine components. Functional applications make use of its unique electrical, optical, and thermal properties for applications used in lasers and low scattering optical windows. Its material properties also afford resistance to breakdown from radiation providing opportunities for space applications. Constructional sapphire is used for creation of products with high mechanical stability such as the supports for the crucible used in the growth of other crystals. Other uses include shatter resistant windows and insulator substrates layers for high power, high frequency complimentary metal oxide semiconductor (CMOS) integrated circuits.[2]

Due to the high melting temperature of sapphire, it is an ideal material for development of optical-based pressure sensors in high temperature operating regimes such as inside gas turbines and embedded in hypersonic aircraft control surfaces. Currently, commercial pressure sensors use silicon on insulator (SOI) technology which requires active cooling to achieve operating temperatures around 1000°C due to the material limitations of silicon. Sapphire based sensors may overcome these limitations; however, this comes with new challenges in the manufacturing process. Sapphire is chemically inert, which precludes the use of standard MEMS etching used in silicon based technologies. To overcome this challenge, an ultra-short pulsed laser machining strategy is employed, but this can lead to microcracking, subsurface damage, residual stress, etc. To minimize these effects, we investigate mechanical behavior post laser machining to better understand ideal manufacturing conditions that produce reliable pressure sensors. An important property of sapphire sensors is the fracture toughness because it affects longevity of components(e.g. a pressure sensor diaphragm). This is investigated using indentation experiments combined with fracture mechanics and single crystal dislocation mechanics.

Fracture properties of sapphire have been studied using indentation to determine its fracture toughness which ranges between 1.5-4.5 MPa$\sqrt{m}$.[3] It was also observed that while studying the basal plane of aluminium oxide that slip and mechanical twinning can be induced when polished or indented with a sharp indenter.[4] Similar finding were found when looking at sapphire using tensile loading at elevated temperatures.[5]

One simple experimental tool for investigating fracture mechanics of brittle materials is micro and nanoindentation.[3] Indentation mechanics has been extensively developed as a way to quantify the hardness of materials. This is done by forcing a small indenter onto the surface of another material and measuring the size of the residual indentation left. It is the most frequently used mechanical test for determining hardness. There are several reasons for implementing this tool including cost, its non-destructive characteristics, and extensions to estimate other mechanical properties from the hardness data.[6] There are several different kinds of indentation including Vicker's, Brinell and Rockwell indenters. One problem with these tests is the lack of a universal methodology to relate hardness calculations from one indent geometry to another. Because hardness is not a well defined parameter, it is often the other mechanical properties such as fracture toughness stated above that are of more interest. Fracture in bulk materials can be characterized using several different techniques including indentation fracture, but there are limited options for use on thin films since it becomes very difficult to differentiate the contributions from each layer. Nanoindentation tests, however, are appropriate at this scale. During these tests, both the displacement and load are monitored during indentation loading and unloading. From this curve, it is possible to estimate the elastic modulus from the unloading curve as well as various other properties such as activation volume and strain rate sensitivity. In the present analysis, we use both micro and indentations to provide more insight into the mechanical behavior of sapphire as a function of single crystal plasticity and laser machining damage.

In the following sections, the methods by which the experimental data was obtained is first discussed followed by results obtained from the data and modeling analysis. We first use anisotropic elasticity (Stroh's formalism[9]) to confirm the crack tip toughness of pristine sapphire. These results are qualitatively compared with toughness enhancements due to laser machining. The experiments are then compared to a finite deformation, dislocation modeling framework to help understand the effect of the damage evolution during indentation loading and unloading. Concluding remarks are given in the final section.

II. Experimental Procedure

Commercially obtained R-plane single crystal sapphire are used in all experiments to support the design of the pressure transducers. Using approximately 9 mm^2 sections of laser machined sapphire we apply Vicker's indentations with a loading force of 1 kg and characterize several indentations. Some of these indentations were made at 0° and 45° relative to the R-plane single crystal cut. Sapphire is non-conductive so a thin layer of carbon was sputtered onto the sample so that it could be observed in a scanning electron microscope (SEM). Crack displacements near the tip were then measured by taking high resolution images near the crack tip.

A 355 nm wavelength picosecond laser was then applied to different specimens to understand how the fracture toughness differed relative to the pristine specimens. The laser itself has 5 different settings that can be adjusted. Those parameters include: the affluence (percentage of the laser power), pulse frequency, scanning speed, number of passes and stepover(indicates the amount of overlap). The laser processing parameters were: 10 kHz pulse frequency, 10 mm/s scanning speed, 3.8 J/cm^2 fluence, 3 passes, and 3 μm stepover. After the specimens are laser machined, we use the same process as before and image the specimens near the indentations in the SEM.

The laser machined specimens are furthered analyzed using a transmission electron microscope (TEM). The TEM (JEM-ARM200cF) is a sub-angstrom spherical aberration corrected transmission/scanning electron microscope. In order to prepare the samples for the TEM, thin slices about 1 mm-2 mm thick were cut using a diamond saw. The slices were polished to about 100 μm using silicon carbide polishing pads starting with 35 μm grit size and finishing with 5 μm grit size gradually stepping down the size as the sample gets thinner. After it is 100 μm thick, the specimen is then attached to a copper grid and polished further using diamond lapping film to a thickness of approximately 20 μm starting with 30 μm grit film and finishing with 1 μm grit film. An ion miller is used in the final step to further polish the sample to a thickness of several nanometers. Images were then obtained at high resolution to observe the effect of the laser machining process.

III. Experimental Results

III.A. Microscopy Results

An example of a SEM image of Vicker's indentations on pristine R-plane sapphire is shown in Figure 1. Cracks are predominately seen emanating from the tips of the indent. We further analyze the pristine specimen by quantifying the crack tip toughness using anisotropic fracture mechanics. We apply Stroh's formalism to determine the K-field associated with the displacement near the crack tip from zoomed SEM images. This approach is done to account for single crystal elastic anisotropy. The details of the approach is well documented elsewhere[9] and therefore not repeated here. By comparing the theoretical displacement to the

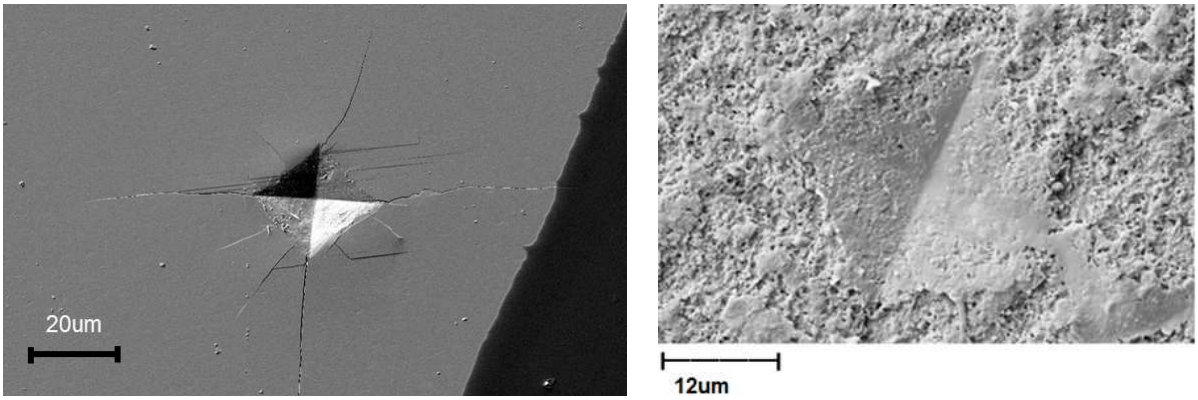

Figure 1. (a) Image of 1 kg indent on pristine sapphire at approximately 0°. (b) Image of 1kg indent on laser machined sapphire at approximately 0°. The laser processing parameters were: 10 kHz pulse frequency, 10 mm/s scanning speed, 3.8 J/cm^2 fluence, 3 passes, 3 μm stepover.

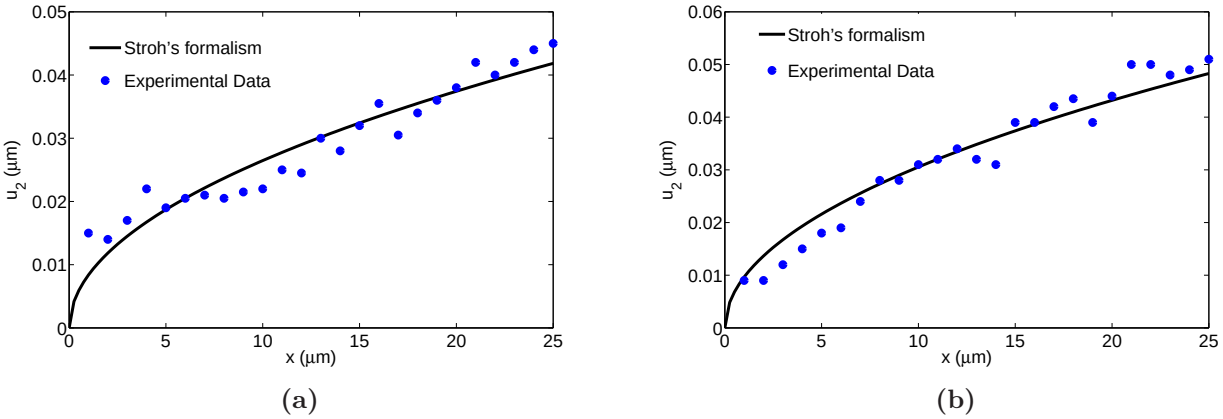

Figure 2. (a) Graph of experimental data matched to theoretical crack displacement for indents oriented at 0° relative to the R-plane. (b) Similar analysis for indents oriented at 45° relative to the R-plane.

crack tip displacements obtained from SEM images, an estimate of the crack tip toughness can be determined as is shown Figure 2. It was found that at 0° the K_{Ic} was 2.2 MPa-m$^{1/2}$ and at 45° it was 2.50 MPa-m$^{1/2}$. The corresponding energy release rates were 11.64$\frac{N}{m}$ and 15.25 $\frac{N}{m}$, respectively. These fracture toughness values are comparable to ones given by Lawn[3] for sapphire which is between 1.5-4.5 MPa-m$^{1/2}$. Because of this wide range it is unclear if the anisotropy has an effect on the fracture toughness.

A comparison of the pristine specimens to the laser machined specimens illustrated toughening upon laser machining as shown in Figure 1(b). No apparent crack formation was observed using picosecond laser machining. Since the fracture toughness could not be determined from indentations, TEM images were investigated to quantify if subsurface damage was present and contributing to the enhanced toughness.

Through the use of TEM imaging, we identified characteristics of laser damage as shown in Figure 3.

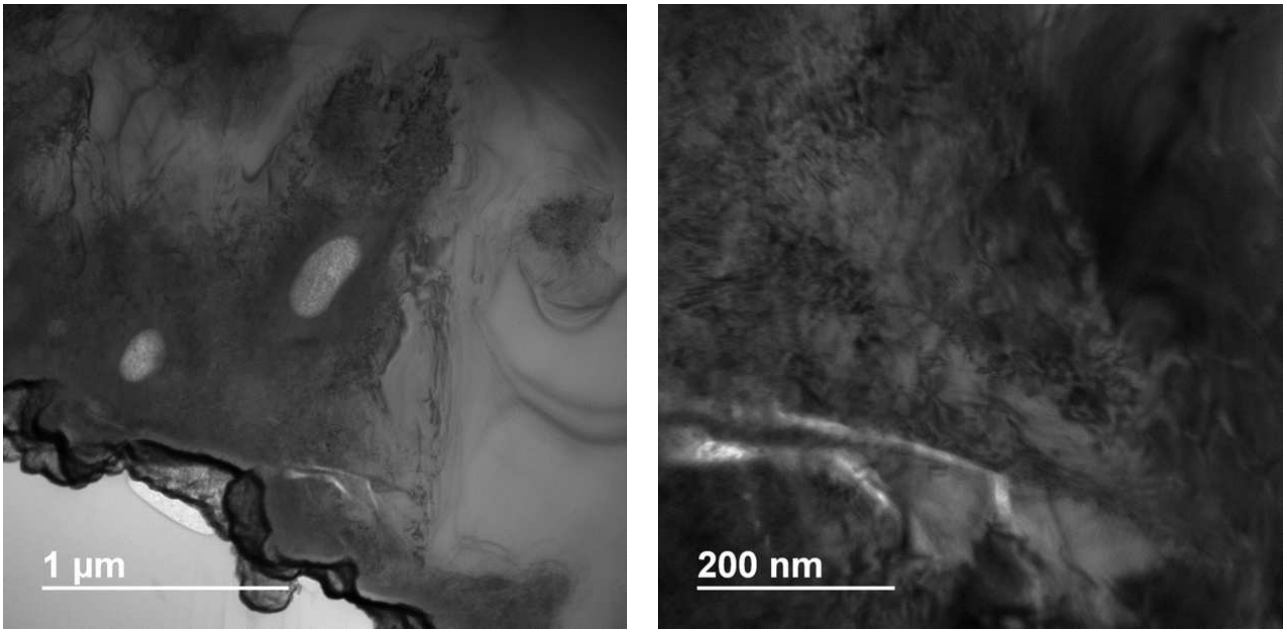

Figure 3. (a) Image of region near the surface showing high density dislocation regions at varying depths in the sapphire with the laser machine parameters: 200 kHz pulse frequency, 200 mm/s scanning speed, 3.8 J/cm^2 fluence, 3 passes, 3 μm stepover. (b) Higher magnification of high density dislocation region with the laser machine parameters: 200 kHz pulse frequency, 200 mm/s scanning speed, 3.8 J/cm^2 fluence, 3 passes, 3 μm stepover.

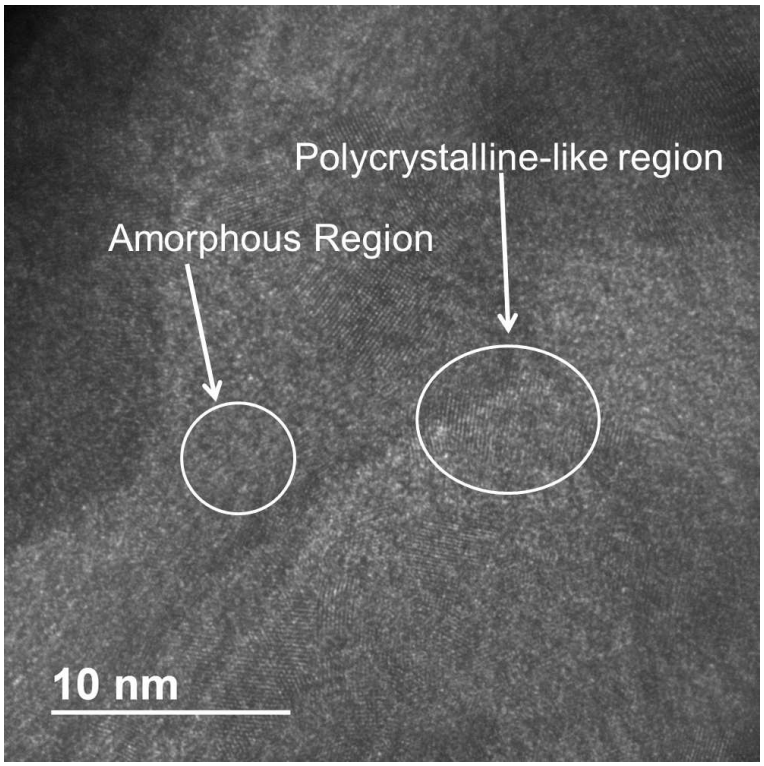

Figure 4. High Magnification region near the surface of the sample showing polycrystalline-like behaviour.

From tilting the TEM sample, the darker regions in Figure 3 were shown to contain regions of highly dense dislocations. The depth of damage ranges from a few hundred nanometers to 5 μm. An interesting phenomenon was observed when viewing the sample at 10s of nm close to the surface. It can be seen in Figure 4 that there are island-like regions where striations can be seen. These regions are indicative of polycrystalline-like behaviour. It is unclear if grain boundaries have formed in the sapphire specimen near its surface. In addition, the regions surrounding the polycrystalline-like areas are believed to be amorphous. These regions are only found within the first 5 nm from the laser machined surface.

IV. Nanoindentation Model

Based on the electron microscopy and indentation results, a damage model was formulated and numerically implemented using the finite element method to better understand the material physics behind deformation in pristine single crystal sapphire for future extensions to initial conditions containing laser machining damage. Aspects of the model governing the evolution of plasticity are adopted from finite single crystal plasticity theory.[10] In the model, a free energy function $\psi = \psi(E_{IJ}, \rho, \rho_{,I})$ is implemented. This free energy is a function of the Lagrangian strain E_{IJ}, a damage parameter ρ associated with dislocation evolution, and its spatial gradient $\rho_{,I}$. To fit our model, we use experimental data from a nano-indentation test and compare the force displacement curves from our simulation to those obtained from the experiment.

IV.A. Governing Equations

It was determined numerically that the strain underneath the indentation was finite so the second Piola-Kirchoff stress is implemented in the equilibrium equations in the Lagrangian frame.[12] This is provided by

$$\tilde{T}_{JI,J} = 0 \tag{1}$$

where body forces and inertial effects are neglected.

The equilibrium equations are coupled to a phase field equation describing dislocation evolution in the single crystal material using

$$\xi_{I,I} - (\eta - \tau) = \beta\dot{\rho} \tag{2}$$

which estimates dislocation evolution using the scalar parameter ρ. In this equation, $\xi_{I,I}$ governs the diffusion length between damage zones and pristine material, η is the internal microscopic force that must be overcome to induce damage, τ is the resolved shear on the slip plane, and β is an inverse mobility constant that accommodates losses proportional to the time rate of change of the damage, $\dot{\rho}$.

The diffusion of damage is governed by

$$\xi_I = a_0\rho_{,I} \tag{3}$$

where a_0 is a phenomenological parameter that is proportional to the diffusion length. The internal microscopic force η is work conjugate to ρ and defined by

$$\eta = \frac{\partial\psi}{\partial\rho} = A\rho + B\rho^3 \tag{4}$$

and the driving force for evolution of the damage parameter is

$$\tau = D\tilde{T}_{IJ}\tilde{s}_I\tilde{m}_J \tag{5}$$

where A,B, and D are phenomenological parameters, s_I is the slip direction,and m_J is the normal associated with the slip plane. In general, this may be extended to multiple slip systems to quantify nonlinear constitutive behavior near the onset of plasticity where multiple slip planes may be activated near the same magnitude of the driving force. Here, we only approximate this behavior by setting the slip direction to 45° for a conical indenter using an axisymmetric model in two dimensions. The approximates the true evolution of dislocation evolution along multiple slip systems in three dimensions. It will be shown this this provides a reasonable estimation of nonlinear deformation and hysteresis during nanoindention of pristine sapphire.

Since we accommodate finite deformation, it is not possible to use a simple linear superposition of the elastic and plastic strain. A multiplicative decomposition of elastic and plastic deformation is alternatively used where the total deformation gradient is $\mathbf{F}=\mathbf{F}^e\mathbf{F}^p$ where $\mathbf{F}^e$ and $\mathbf{F}^p$ are the elastic and plastic deformation gradient tensors.[10,13] This results in another set of unknown plastic deformation gradient components that are determined as a function of the damage parameter ρ. Following Gurtin et al.,[10] we introduce the kinematic relation

$$\dot{F}^p_{iK} - \dot{\rho}(s_i m_j)F^p_{jK} = 0 \tag{6}$$

which provides a means to determine components of the plastic deformation gradient F^p_{iK}. In summary, the three governing equations (1), (2), and (6) are solved simultaneously with the finite element method.

V. Computational Modeling

The software Comsol was used to solve the nonlinear set of solid mechanics equations. The model was developed in two dimensions by assuming axisymmetric deformation. The strong forms of the governing equations (1) and (2) are rewritten in the weak form and specified for the axisymmetric case. Starting with (1) the final weakform is

$$\int_\Omega -[(\frac{\partial w_r}{\partial r}\tilde{T}_{rr} + \frac{\partial w_r}{\partial z}\tilde{T}_{rz})r^2 + (\tilde{T}_{rr} + \tilde{T}_{zz})rw_r]d\Omega + \int_\Gamma[(\tilde{T}_{rr} + \tilde{T}_{rz})r^2 n_r w_r]d\Gamma = 0 \tag{7}$$

$$\int_\Omega -[(\frac{\partial w_z}{\partial r}\tilde{T}_{rz} + \frac{\partial w_z}{\partial z}\tilde{T}_{zz})r]d\Omega + \int_\Gamma[(\tilde{T}_{rz} + \tilde{T}_{zz})rn_z w_z]d\Gamma = 0 \tag{8}$$

where w_r and w_z are weight functions for the displacement variables in the radial (w_r) and z-direction (w_z). Both (2) and (6) are implicitly defined in the coordinate system by their variables. The weak form for (2) is

$$\int_\Omega[\xi_I w_{,I} - (\eta - \tau - \beta\dot{\rho})w_\rho]d\Omega + \int_\Gamma[w_\rho\xi_I n_I]d\Gamma = 0 \tag{9}$$

where w_ρ is the weight function on the damage parameter and the diffusion variable becomes $\frac{\xi_r}{r} + \xi_r$ and ξ_z in the radial and z-directions, respectively. The weak form for the plastic deformation tensor is

$$\int_\Omega [(\dot{F}_{iK} - \dot{\rho}(s_i m_j F_{jK}))w_{iK}]d\Omega = 0 \tag{10}$$

Here w_{iK} is the weight function on each of the non-zero components of the finite plastic deformation gradient. It is important to note that the dependent variable u (displacement in the radial direction) in the definitions of the strains used in the model is $\frac{u}{r}$ in order to avoid a singularity at $r = 0$.

The two-dimensional geometry is a rectangle with dimensions 300 μm x 500 μm in the r and z directions, respectively. The boundary conditions are illustrated in Figure 5(a). Axisymmetric boundary conditions are applied along the $r = 0$ axis (left side in Figure 5(a)) and a fixed displacement is applied along the bottom of the model. It has been shown that a Berkovich indentation can be approximated by an equivalent conical indentation so that axisymmetry can be utilized.[11] For this model, the elastic and plastic properties were assumed to be isotropic so that the symmetry condition is not violated. The load P along the contact surface of the indent is solved according to the difference between a prescribed indentation displacement and the finite element solution and described as follows. Using this approach, the displacments of the finite element model reasonably follow the indent geometry except near the center point of the indent as shown in Figure 5(b).

There is also a special boundary condition implemented along the top to approximate the contact mechanics of a Berkovich indenter. A virtual indentation is applied to the material to simplify the contact problem. This is accomplished by applying a load boundary condition on the top surface which depends on the difference between the prescribed displacement from the virtual indent contacting surface and the actual surface displacement from the finite element model solution

$$F_z = k(v_{FEA} - v_{pre})r \tag{11}$$

where k is a spring stiffness parameter that can be increased to minimize the difference between the FEA surface displacements (v_{FEA}) and the prescribed indent displacement (v_{pre}). Due to stability issues, there is a limit as to how large the spring constant can be increased. The indentation depth used to construct v_{pre} is larger than the true indent geometry such that the maximum displacement of v_{FEA} matches results from nanoindentation data. In order to avoid the un-physical phenomenon of a tensile load along the boundary between contact and a free surface, a constraint is implemented so that the spring forces are never tensile.

Upon numerical implementation and comparison with nanoindentation data, it was determined that the amount of hysteresis observed experimentally could not match data without significantly decreasing the

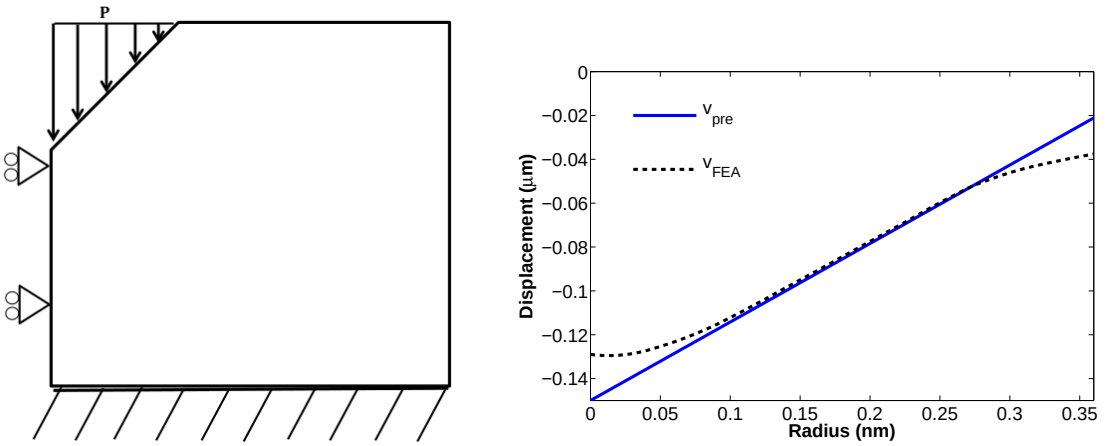

(a) (b)

Figure 5. (a) Boundary conditions applied to finite element model. There is zero displacement in the r direction along the axis of symmetry and fixed along the bottom. There is then a virtual indentation applied on the top with a load. (b) Graph of difference in the prescribed displacement and actual displacement in the model.

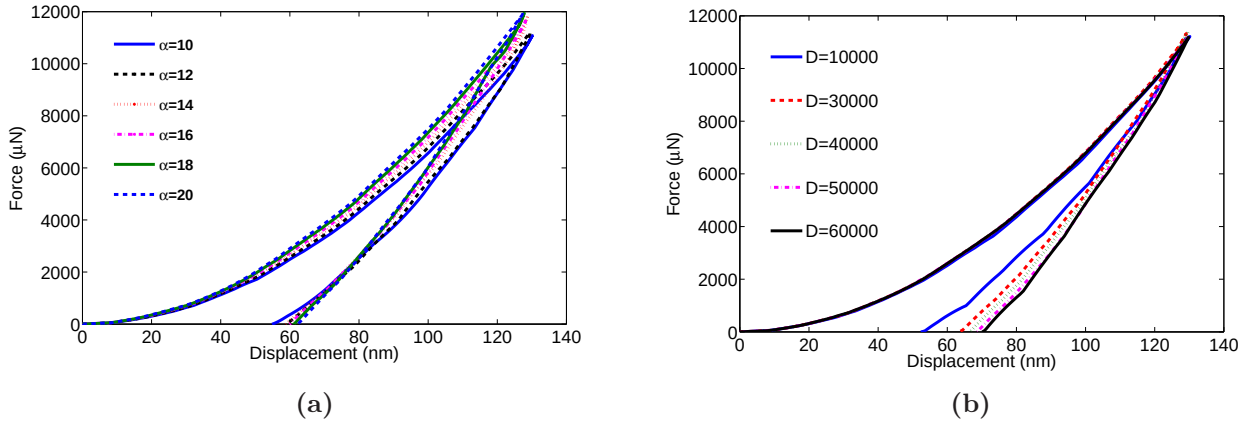

Figure 6. (a) As α increases the peak load increases while keeping the hysteresis relatively constant. (b) As D increases the peak load stays almost the same while being able to increase the hysteresis in the force displacement curve.

maximum load. In order to match both the hysteresis and maximum load, the shear modulus was assumed to increase as a function of the damage according to

$$G = G_0(1 + \alpha\rho^2). \tag{12}$$

This allowed for the max load to remain relatively constant as the amount of damage and subsequently, the hysteresis, increased such that it could be matched to experimental results.

To better understand the effects of the model parameters, a local sensitivity analysis was conducted. It was determined that the magnitude of parameters A and B strongly influence model stability and also influence the amount of hysteresis. Once model stability was achieved, it was possible to fit data by holding A and B constant and varying α and D. It can be seen in Figure 6 how the curves are affected by changing one parameter while the other parameters are held fixed. The trend for both parameters is as expected. As α increases, so does the maximum load and as D increases, so does the amount of hysteresis.

An example of one of the FEA solutions is shown in Figure 7. It can be seen that there is permanent

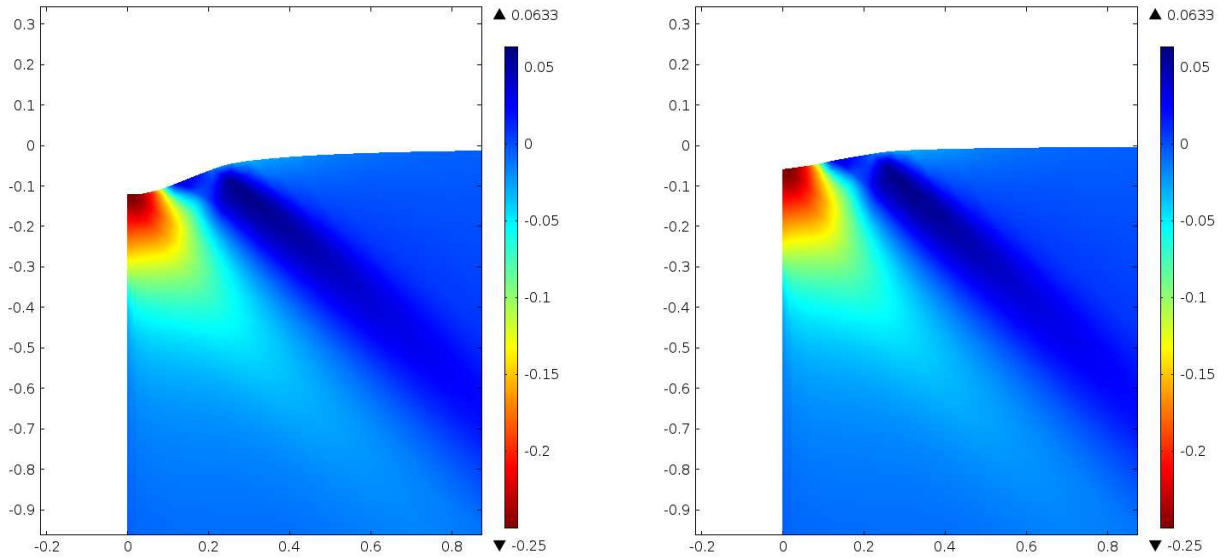

Figure 7. (a) The FEA solution showing the plastic strain in the z direction (E^p_{zz}) at the maximum load. (b) The FEA solution illustrating the residual E^p_{zz} after the load has been removed.

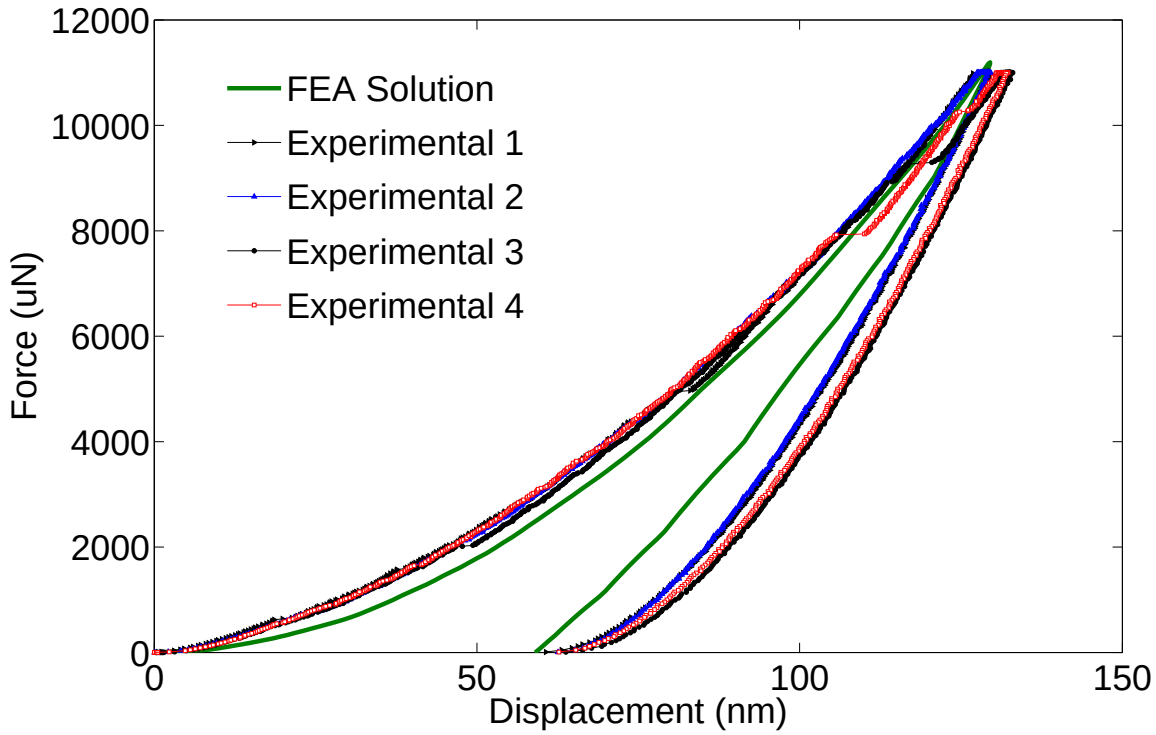

Figure 8. Comparison of force displacement curves from nanoindentation experiment and numerical simulation

deformation after the load is completely removed as indicated by the remanent deformation and color plot of plastic strain in the z-direction, E_{zz}. This is also shown in the load-displacement curve for one set of parameters in Figure 8. Since the phenomenological parameters A, B, and D all have a significant influence on damage evolution but not hardening, this provides evidence that the increase in elastic properties (here proposed to be the shear modulus G in Eq. (12)) is a strong indication that there are two mechanisms occuring during the indentation process.

VI. Conclusion

Materials characterization and modeling of both pristine and laser machined specimens has illustrated that laser machining has significant effects on the fracture behavior and subsurface damage. The laser machining is found to toughen the sapphire. It appears that this is due to the high density dislocation region caused by the laser machining process which vary in depth from 0.5 μm to 5 μm. To better understand this behavior in brittle single crystal materials, a model was developed using a scalar order parameter to approximate dislocation formation and evolution. It was assumed that the majority of slip occurred at 45^o to the R-plane crystal surface. This phenomenological model illustrated that parameters associated with changes in the elastic properties (via α) and the amount of plasticity (via D) are most sensitive to fit the model where the other two parameters associated with dislocation energetics (A and B) are important for numerical stability. From the results of the simulations, we conclude that there are two mechanisms governing deformation during nanoindentation of pristine sapphire. The first is the compression of the atomic structure causing an effective hardening that can be associated with a localized increase in the shear modulus. The second is the formulation of plasticity when the local stresses becomes to large and it is more energetically favourable for slip to occur. Current research is focused on extending this research to understand nanomechanics when dislocations are initially present from laser machining.

Acknowledgments

The authors would like to thank the FAA (Grant: CA 10-C-CST-FSU) and the DOE (Grant: FE0012370) for providing funds to support this research. J. Collins would also like to thank the Aero-propulsion, Mechatronics, and Energy Center for support through a fellowship. The authors are also very thankful for help Dr. Yan Xi provided in using the TEM located at the National High Magnetic Field Laboratory at Florida State University.

References

[1]M. Yoshioka *Plastically deformed region around indentations on si single crystal* Journal of Applied Physics, vol. 76, no. 12, pp. 7790-7796, 1194.

[2]Elena R. Dobrovinskaya, Leonid A. Lytvynov, Valerian Pishchik *Sapphire Material, Manufacturing, Applications* 2009: Springer Science+Business Media.

[3]Brian Lawn *Fracture of Brittle Solids* 1993: Cambridge University Press, 2nd ed.

[4]Bernard J. Hockey *Plastic Deformation of Aluminum Oxide by Indentation and Abrasion* Journal of the American Ceramic Society Vol.54, No.5 1971.

[5]M.L. Kronberg *Plastic Deformation of Single Crystals of Sapphire: Basal Slip and Twinning* Acta Metallurgica, Vol. 5, 1957.

[6]William D. Callister, Jr. *Material Science and Engineering An Introduction*.

[7]R. Kienzler, G. Herrmann *On the properties of the Eshelby tensor* Acta Mechanica 125, 73-91 (1997).

[8]J.W. Eishen *Fracture of nonhomogenous materials* International Journal of Fracture 34, 3-22 (1987).

[9]Ting, T. C.-t. *Anisotropic Elasticity Theory and Applications* New York: Oxford UP, 1996. Print.

[10]Gurtin, Morton E., Eliot Fried, and Lallit Anand. *The Mechanics And Thermodynamics Of Continua* New York: Cambridge UP, 2010. Print.

[11]A.C. Fischer-Cripps *Nanoindentation* 2004, New York: Springer.

[12]Lawrence E. Malvern *Introduction To The Mechanics Of Continuous Medium* Englewood Cliffs, NJ: Prentice-Hall, 1969. Print.

[13]Maugin,G. A. *Configurational Forces: Thermomechanics, Physics, Mathematics and Numerics* Boca Raton Chapman and Hall/CRC, 2010. Print.